PCCP

Cite this: *Phys. Chem. Chem. Phys.*, 2012, **14**, 1876–1880

www.rsc.org/pccp

PAPER

Mechanism of photocatalytic activities in Cr-doped $SrTiO_3$ under visible-light irradiation: an insight from hybrid density-functional calculations†

Pakpoom Reunchan,[a] Naoto Umezawa,*[ab] Shuxin Ouyang[a] and Jinhua Ye[ac]

Received 23rd October 2011, Accepted 29th November 2011
DOI: 10.1039/c2cp23348g

We used hybrid density-functional calculations to clarify the effect of substituting chromium for titanium (Cr_{Ti}) on photocatalytic activities of Cr-doped $SrTiO_3$. A singly negative Cr_{Ti}^{-}, which is relevant to a lower oxidation state of Cr, is advantageous for the visible light absorption without forming electron trapping centers, while other charge states are inactive for the photocatalytic reaction. Stabilizing the desirable charge state (Cr_{Ti}^{-}) is feasible by shifting the Fermi level towards the conduction band. Our theory sheds light on the photocatalytic properties of metal-doped semiconductors.

1. Introduction

Photocatalysis has attracted much attention for its potential applications in environmental purification and fuel production. Since the discovery of water splitting on the surface of TiO_2,[1] the photocatalytic properties of various metal oxide semiconductors have been extensively studied.[2] The oxides such as ZnO, SnO_2 and $SrTiO_3$ have a wide-band gap and possess suitable band structures to act as photocatalysts:[3] the positions of the valence band (VB) and conduction band (CB) edges are appropriate for oxidation and reduction reactions of water and organic molecules. Perovskite $SrTiO_3$ has characteristics that are useful for photoelectrolysis, such as high chemical stability. It has a CB edge that is 0.8 eV higher than the standard hydrogen electrode potential,[4] making its reducing power stronger than that of TiO_2 under ultraviolet (UV) irradiation without any bias voltage,[5,6] and in principle, it can be used for overall water splitting.[7] However, $SrTiO_3$ can absorb radiation only from the UV portion of the solar spectrum, because it has a large energy gap of about 3.2 eV that hinders the efficiency of solar-energy conversion. Great efforts have therefore been made to reduce the energy gap of $SrTiO_3$. One approach is to shift the VB upwards into the visible range of its band gap, while keeping the CB edge intact in order to maintain its ability to reduce water to hydrogen (H_2). A doping strategy with either cations[8–14] or anions[15,16] has been widely adopted for this purpose.

Chromium doping is one successful example of this approach for enhancing visible-light absorption in both TiO_2 and $SrTiO_3$.[8,9,11–14] Its effects on the photocatalytic production of H_2 and O_2 by water splitting, as well as the photocatalytic decomposition of organic compounds, have been widely studied. Experimental results have revealed that Cr-doping is effective for the evolution of H_2 but not O_2 under visible light; this suggests that Cr-related discrete states are formed above valence-band maximum (VBM) without any change to the CB edge. X-Ray photoelectron spectroscopic (XPS) measurements showed that the photocatalytic activity was enhanced by the presence of trivalent Cr ions (Cr^{3+}), but diminished by the presence of hexavalent Cr (Cr^{6+}).[12,13] In addition, experimental results showed that codoping with donor-type impurities and/or H_2 reduction treatment could enhance the photocatalytic H_2 evolution in Cr-doped $SrTiO_3$,[11,13] indicating that an *n*-type environment, in which the Fermi level is located near the conduction-band minimum (CBM), is advantageous for stabilizing Cr^{3+}. First-principles calculations have been previously carried out for Cr-doped $SrTiO_3$;[17] however, the relationship between the oxidation state of Cr and photocatalytic activity remains unclear. Although transition-metal impurities in various semiconductors have been extensively studied in the contexts of defect physics,[18] magnetism,[19,20] and superconductivity,[21] their role in photocatalysis has not been clarified.

The present article demonstrates that the oxidation state of Cr drastically affects the electronic structure of Cr-doped $SrTiO_3$ using screened hybrid density-functional calculations. It is energetically favorable for Cr impurities to occupy the Ti site under any equilibrium growth conditions; Cr_{Ti} is therefore likely to be responsible for visible-light absorption and photocatalytic enhancement in Cr-doped $SrTiO_3$. Under *n*-type

[a] *The Research Unit for Environmental Remediation Materials, National Institute for Materials Sciences, Ibaraki 305-0047, Japan. E-mail: umezawa.naoto@nims.go.jp*
[b] *PRESTO, Japan Science and Technology Agency (JST), 4-1-8 Honcho Kawaguchi, Saitama 332-0012, Japan*
[c] *International Center for Materials Nanoarchitectonics (MANA), National Institute for Materials Sciences, Ibaraki 305-0047, Japan*

† Electronic supplementary information (ESI) available: (1) density of states (DOS) for Cr_{Ti}, (2) description of the role of Cr_i, and (3) calculation details for the absorption and emission at Cr_{Ti}^{0}. See DOI: 10.1039/c2cp23348g

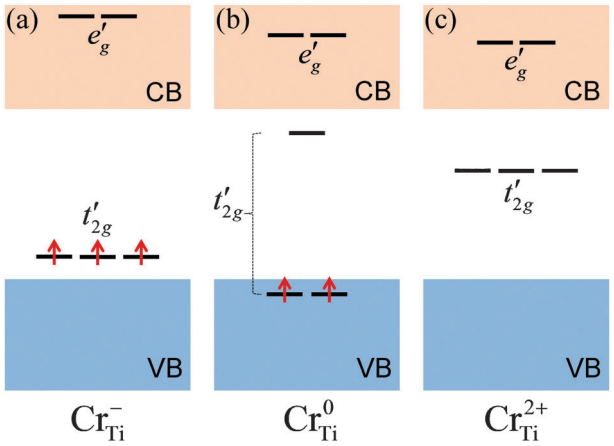

Fig. 1 Schematic illustrations of *d* states single-particle energy levels of the Cr_{Ti} in the band gap for (a) –, (b) neutral, and (c) 2+ charge states in the spin-up channel. The arrows show the electron occupation, corresponding to the associated charge state.

conditions, Cr_{Ti} becomes an acceptor; it is present in the negative charge state (Cr_{Ti}^{-}), in which the Cr t_{2g}-derived states (t'_{2g}) are fully occupied (Fig. 1(a)). These occupied states are located in the band gap and act as electron sources for photoexcitation, causing a red shift of the photoabsorption edge. When the Fermi level is lower, Cr_{Ti} is present in the neutral charge state (Cr_{Ti}^{0}), and the t'_{2g} states are split and partially occupied (Fig. 1(b)). By contrast, under *p*-type conditions in which the Fermi level is located near the VBM, Cr_{Ti} is present in the 2+ charge state (Cr_{Ti}^{2+}), rendering the Cr t'_{2g} states empty in the band gap (Fig. 1(c)). This drastic change of the electronic structure is predicted to be responsible for the strong dependence of the photocatalytic activities on synthetic processes. Our theoretical study not only systematically explains the recent experimental results[11–13] but also provides a strategy for developing metal-doped semiconductor photocatalysts by controlling the desired growth/synthetic conditions that stabilize the active doped-metal-ions.

2. Computational methods

Our calculations are based on density functional theory, as implemented in the VASP code,[22] with the Heyd, Scuseria, and Ernzerhof (HSE) hybrid functional.[23] The Coulomb potential in the exchange energy is divided into short-range and long-range parts in the HSE approach with a screening length of 10 Å. In the short-range part, the non-local Hartree–Fock (HF) exchange is mixed with the Perdew, Burke, and Ernzerhof (PBE) generalized-gradient approximation (GGA) exchange energy.[24] The long-range part and correlation potential are represented by the PBE functional. The HF mixing parameter of 28% gives good agreement with the experimental band gap of $SrTiO_3$.[25] Using HSE to reproduce the correct band gap yields an accurate description of the electronic structure and formation energies of defects in oxide semiconductors.[26] The calculated lattice constant of $SrTiO_3$ (space group $Pm\bar{3}m$) a = 3.913 Å is in good agreement with the experimental value (3.905 Å).[27] The Sr $4s^2 4p^6 5s^2$, Ti $3d^3 4s^1$, and the Cr $3s^2 3p^6 3d^5 4s^1$ states are treated as valence states. The energy cutoff of 400 eV is used for the planewave expansion. Our calculations of defects use a (3 × 3 × 2) 90-atom supercell and a 2 × 2 × 2 grid of Monkhorst–Pack *k*-point set for the Brillouin zone integration. Test calculations using 40- and 135-atom supercells show that our main conclusion is not affected by the supercell size. All calculations involving unpaired electrons are spin-polarized.

To identify the dominant form of the Cr impurity in $SrTiO_3$, we compared the stability of Cr at the Ti site (Cr_{Ti}), the Sr site (Cr_{Sr}), and the interstitial site (Cr_i). The likelihood of incorporation of an impurity in $SrTiO_3$ was determined by its formation energy. The formation energy of a Cr atom occupying the site X in the charge state q is defined as:

$$E^f(Cr_X^q) = E_{tot}(Cr_X^q) - E_{tot}(SrTiO_3) + \mu_X - \mu_{Cr} + q\varepsilon_F, \quad (1)$$

where $E_{tot}(Cr_X^q)$ is the total energy of a $SrTiO_3$ supercell containing one Cr at an X site (X = Sr or Ti, μ_X = 0 for Cr_i) and $E_{tot}(SrTiO_3)$ is the total energy of a perfect $SrTiO_3$ in the same supercell. ε_F is the Fermi level referenced to the bulk VBM, which represents the energy of the electron reservoir for charged impurities. We have not applied Madelung corrections for the fictitious electrostatic interactions between the charged defect and the homogenous background charge, because the static dielectric constant of $SrTiO_3$ is relatively large.[28] The X atom that is removed from the supercell for substituting Cr is placed in the reservoir of energy μ_X.

The chemical potential plays an important role in our analysis and must be carefully chosen to avoid improper conclusions.[29] In an equilibrium growth condition of $SrTiO_3$, the chemical potentials must satisfy the relation $\mu_{Sr} + \mu_{Ti} + 3\mu_O = \mu_{SrTiO_3} = -16.2$ eV where the atomic chemical potential is defined as the energy referenced to its value in the elemental phase. Indeed, each of the atomic chemical potential must possess a negative value to avoid the formation of metallic Sr, Ti, or O_2 gas. In addition, we must enforce the constraints such as $\mu_{Sr} + \mu_O < \mu_{SrO}$, to prevent the precipitation of SrO during the growing process of $SrTiO_3$. The similar constraints must be applied to the other relevant compounds: SrO_2, TiO, TiO_2, and Ti_2O_3. These constraints define a domain in a two dimensional coordinate consisting of μ_{Ti} and μ_{Sr} axes shown as a filled area in Fig. 2. μ_{Ti} and μ_{Sr} are allowed to vary only within the domain and μ_O is uniquely determined by the equilibrium condition above. The domain ensures that $SrTiO_3$ grows without transition to the other phases, and thus any equilibrium experimental growth or annealing conditions must correspond to somewhere in this domain. We selected three different chemical potential settings (μ_{Sr}, μ_{Ti}, μ_O), corresponding to the solid circles in Fig. 2: (a) O-poor condition (−0.38, 0, −5.27), (b) the intermediate condition $\mu = \mu_{Cr/Sr}$ (−3.59, −2.34, −3.42), and (c) the relative Ti/Sr-poor $\mu = \mu_{Cr/Ti}$ (−5.41, −10.07, −0.24), which are referenced to the values in the elemental phases. The O-poor condition is defined by the position where $\mu_{Ti} + \mu_{Sr}$ has the maximum value in the domain. The $\mu = \mu_{Cr/Sr}$ and $\mu = \mu_{Cr/Ti}$ conditions are established by a set of chemical potentials where $\mu_{Sr} - \mu_{Ti}$ and $\mu_{Ti} - \mu_{Sr}$ have the minimum value in the domain, and therefore, they have the best chance for the Cr atom to substitute for Sr and Ti, respectively. The μ_{Cr} is a

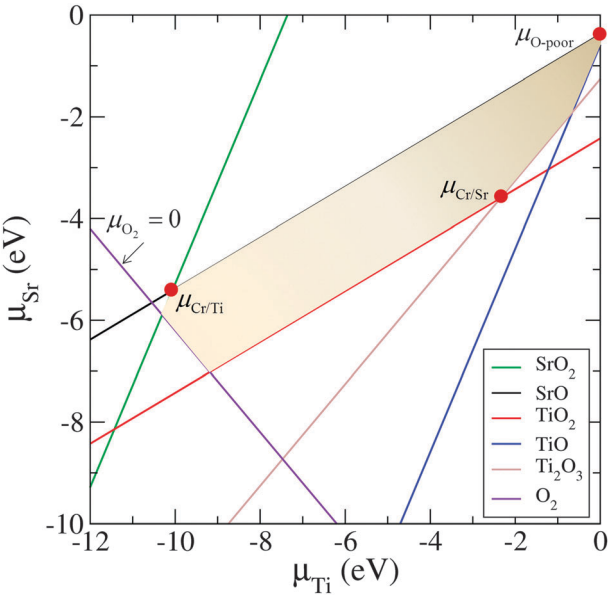

Fig. 2 An illustration of the chemical potential diagram associated with equilibrium growth of $SrTiO_3$. For stable growth of $SrTiO_3$, μ_{Sr} and μ_{Ti} lying in the shaded area are required. The three selected chemical potential settings are shown as solid circles.

set corresponding to its upper bound for each growth condition: it was taken from metallic Cr ($\mu_{Cr} = \mu_{Cr[bulk]}$) for the O-poor condition, Cr_2O_3 ($\mu_{Cr} = (\mu_{Cr_2O_3} - 3\mu_O)/2$) for the $\mu = \mu_{Cr/Sr}$ condition, and CrO_3 ($\mu_{Cr} = (\mu_{CrO_3} - 3\mu_O)$) for the $\mu = \mu_{Cr/Ti}$ condition.

3. Results and discussion

Fig. 3 shows the calculated defect formation energies for the three selected growth conditions. The slope of each line reflects the most stable charge state under the Fermi level conditions. For example, Cr_{Ti} is thermodynamically stable in the 2+, neutral, and − charge states as the Fermi level increases. The thermodynamic transition levels $\varepsilon(q_1/q_2)$[30] for Cr_{Ti}, which are denoted as kinks on each line, are determined as

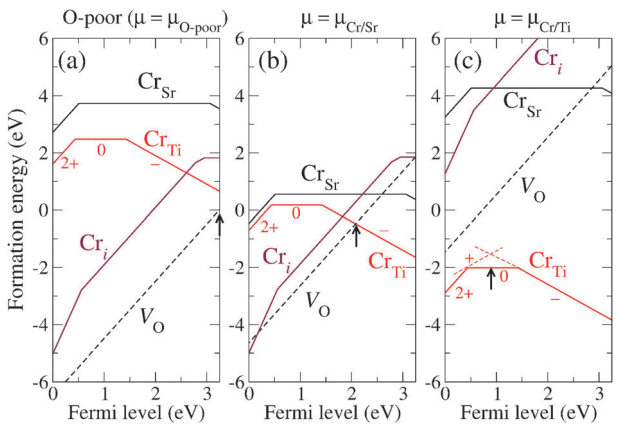

Fig. 3 Calculated formation energy as a function of the Fermi level for Cr-related defects, and the oxygen vacancy (V_O), under (a) O-poor, (b) $\mu = \mu_{Cr/Sr}$, and (c) $\mu = \mu_{Cr/Ti}$ growth conditions. The pinned Fermi level is indicated by the arrow.

$\varepsilon(2+/0) = 0.44$ eV and $\varepsilon(0/-) = 1.43$ eV with respect to the VBM. This suggests that Cr_{Ti} is an amphoteric defect, and can behave as both a donor and an acceptor. Note that the formation energy of Cr_{Ti} is always lower than that of Cr_{Sr} under the examined growth conditions, even when Cr has its best chance to substitute Sr ($\mu = \mu_{Cr/Sr}$).

The Fermi level is determined by a charge balance between donors and acceptors. The most plausible donor that compensates for the Cr_{Ti}^{-} acceptor was found to be the oxygen vacancy (V_O), because it showed sufficiently low formation energy with the 2+ charge state, acting as a double donor (V_O^{2+}) (the role of Cr_i is discussed in the ESI†). Thus, the charge neutrality is satisfied when the concentration of Cr_{Ti}^{-}, which is proportional to the Boltzmann factor $\exp(-E^f(Cr_{Ti}^{-})/k_BT)$, is twice that of V_O^{2+}. This gives a Fermi level that virtually corresponds to the intersection of the two lines for Cr_{Ti} and V_O. Under the O-poor conditions (Fig. 3(a)), the two lines intersect in the CB, so a realistic Fermi-level should be located at the CBM, while under the $\mu = \mu_{Cr/Sr}$ growth conditions (Fig. 3(b)) the Fermi level is located in the band gap at 2.10 eV above the VBM. A typical annealing temperature of 900 °C[12] was used for the Boltzmann factor; however, the choice of temperature does not significantly affect the Fermi level. Under the $\mu = \mu_{Cr/Ti}$ growth conditions (Fig. 3(c)), V_O^{2+} has a higher formation energy than Cr_{Ti}^{+} and Cr_{Ti}^{2+}; thus Cr_{Ti} compensates itself by balancing charges between Cr_{Ti}^{-} acceptor and Cr_{Ti}^{+} (and Cr_{Ti}^{2+}) donors (Fig. 3(c)). The Fermi level is, thus, pinned at about 0.92 eV above the VBM, under which conditions Cr_{Ti}^{0} predominates. The negative value of the formation energy of Cr_{Ti} in the entire range of Fermi energy (Fig. 3(c)) does not indicate that the $SrTiO_3$ sample disintegrates as a result of the impurities; rather, it suggests that Cr_{Ti} is highly stable compared with the other Cr-related defects because the actual chemical potential of Cr should be much lower, making the concentration of Cr_{Ti} relatively low. Notably, V_O^{2+} does not introduce any defect level that traps photoexcited electrons in the gap. The electronic structure of each stable charge state of Cr_{Ti} is schematically illustrated in Fig. 1, which is consistent with the density of states computed for each charge state of Cr_{Ti} (see ESI†). However, Cr_{Ti}^{-} and Cr_{Ti}^{0} predominate under the considered growth conditions, as Cr_{Ti}^{2+} is stable only in *p*-type $SrTiO_3$.

Fig. 4(a) shows the configuration coordinate diagram[30] for the optical transitions initiated by the Cr_{Ti} center. The transitions

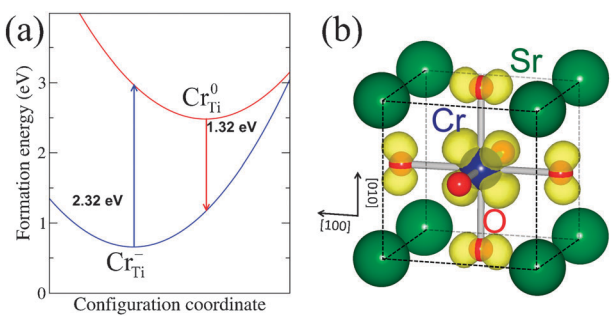

Fig. 4 (a) Configuration-coordinate diagram for the Cr_{Ti} in $SrTiO_3$. The formation energy corresponds to the O-poor condition and to ε_F at the CBM. (b) Spin density of Cr_{Ti}^{-} derived from a t_{2g}' state.

occur through the process $Cr_{Ti}^{-} + h\nu \rightarrow Cr_{Ti}^{0} + e^{-}$ in which Cr_{Ti}^{-} absorbs a photon and is converted to Cr_{Ti}^{0} with an electron in the CB. The absorption energy was, derived from $E^f(Cr_{Ti}^{0};Cr_{Ti}^{-}) - E^f(Cr_{Ti}^{-};Cr_{Ti}^{-})$, where $E^f(Cr_{Ti}^{q1};Cr_{Ti}^{q2})$ denotes the formation energy of Cr_{Ti}^{q1} with the geometry relaxed for Cr_{Ti}^{q2}. The absorption energy was found to be 2.32 eV, which was in good agreement with the photoabsorption edge observed in experiments at 530 nm (2.34 eV).[12–14] Hence, the visible-light absorption in Cr-doped $SrTiO_3$ is likely to be attributable to this photoexcitation process. The photoabsorption at Cr_{Ti} is accompanied by a photoexcited electron that is drawn from an in-gap t'_{2g} state and raised to the CBM. The occupied t'_{2g} states for Cr_{Ti}^{-} are localized around the Cr_{Ti} site (Fig. 4(b)); in other words, the absorption occurs *via* an optical transition between a discrete impurity-level and the CB, rather than a band-to-band transition with a narrowed band gap. The photoexcited holes are thus expected to be trapped at the Cr_{Ti} center, thereby losing their mobility. This is consistent with the results of photocatalytic experiments on Sb and Cr codoped $SrTiO_3$, which found the O_2 evolutions to be much smaller than the H_2 evolution.[11] In addition, the energy difference corresponding to photoemission (when an electron in CB is recombined with a hole trapped at Cr_{Ti}^{-}) can be computed from $E^f(Cr_{Ti}^{0};Cr_{Ti}^{0}) - E^f(Cr_{Ti}^{-};Cr_{Ti}^{0}) = 1.32$ eV (Fig. 4(a)). The energy difference between absorption (2.32 eV) and emission (1.32 eV) reflects the Stokes shift; that is the emitted photon has less energy than the absorbed photon due to the difference in local lattice relaxations of Cr_{Ti}^{-} and Cr_{Ti}^{0}. This result agrees with those of photoluminescence experiments performed on Sb and Cr codoped and Cr^{3+} doped $SrTiO_3$ in which the emission occurred at about 800 nm (1.55 eV).[11] Analogous analysis of optical transition for the process $Cr_{Ti}^{0} + h\nu \rightarrow Cr_{Ti}^{-} + h^{+}$ yields an absorption energy of 1.93 eV and emission energy of 0.93 eV (see ESI†). This suggests that the higher oxidation state of Cr_{Ti} (Cr_{Ti}^{0}) can also have an effect on visible light; however it cannot enhance H_2 evolution because the unoccupied state in the band gap can act as an electron trapping center (Fig. 1(b)), thereby degrading the reduction process. This result is consistent with the observation in ref. 12 that the higher oxidation state of Cr was disadvantageous for the photocatalytic reaction even though visible-light absorption was enhanced.

To relate the stable charge states of Cr_{Ti} to the oxidation state, we analyzed the Bader charge[31] of Cr ions in Cr_{Ti}^{-}, Cr_{Ti}^{0}, and Cr_{Ti}^{2+} compared with that in CrO_3, CrO_2 and Cr_2O_3. The results are summarized in Table 1 along with the average Cr–O bond lengths. The Bader charge on the Cr atom in CrO_3 was larger than those in CrO_2 and Cr_2O_3, consistent with the formal oxidation states (Cr^{6+}, Cr^{4+} and Cr^{3+}, respectively). The Bader charges for Cr_{Ti}^{2+} (+2.26), Cr_{Ti}^{0} (+2.05) and Cr_{Ti}^{-} (+1.91) were similar to those for CrO_3 (+2.25), CrO_2 (+2.06) and Cr_2O_3 (+1.82), respectively. This suggests that the oxidation states of Cr_{Ti}^{-}, Cr_{Ti}^{0}, and Cr_{Ti}^{2+} are possibly 3+, 4+, and 6+, respectively. In addition, this is qualitatively consistent with the charge-self regulation hypothesis,[18] which argues that the net charge transfer to or from a transition-metal atom in insulators (Cr_{Ti} in our case) is negligible, and that the change in the metal (Cr) oxidation state is attributable to the occupation of the in-gap crystal field resonance (CFR) level (that is t'_{2g} states in our case). The increase in the Cr–O bond length as more t'_{2g} states are occupied indicates the anti-bonding characteristics of such states.

Table 1 Calculated Bader charges for Cr in Cr_2O_3, CrO_2, and CrO_3, and for substitutional Cr_{Ti} in charge state q. The average Cr–O bond lengths are also listed. The values in parentheses are the difference from the equilibrium Ti–O bond length

Structure/defect	q	Cr charge (electrons)	Cr–O bond length/Å
Cr_2O_3		+1.82	1.95
CrO_2		+2.06	1.97
CrO_3		+2.25	1.64
Cr_{Ti}	−	+1.91	1.98(+1.0%)
	0	+2.05	1.92(−2.0%)
	+	+2.15	1.90(−3.1%)
	2+	+2.26	1.85(−5.6%)

Our results indicate that the oxidation state of chromium impurities, and thereby the photocatalytic activity, can be influenced by the growth conditions and the Fermi level of the system. According to our analysis Cr_{Ti}^{-}, which is likely to be Cr^{3+}, is advantageous for the visible-light absorption and H_2 evolution because it gives rise to occupied t'_{2g} states above the VBM (Fig. 1(a)) without forming electron-trapping centers near the CBM. This is consistent with recent experiments showing that the Cr-doped $SrTiO_3$ samples that contain Cr^{3+} exhibit relatively high photocatalytic activities under visible light, whereas samples with the higher oxidation state of Cr are inactive.[12,13] Our theory suggests that the desirable charge state of Cr_{Ti}^{-} can be stabilized by synthesizing the sample in an appropriate environment in which the chemical potentials are close to the O-poor or $\mu = \mu_{Cr/Sr}$ conditions (Fig. 3(a) and (b)). Alternatively, one can shift the Fermi level upwards near the CBM by codoping with donor-type impurities, because Cr_{Ti}^{-} will predominate under any growth conditions and under these circumstances (Fig. 3). This could also explain why the photocatalytic performance of Cr-doped $SrTiO_3$ is improved by doping with Sb, Nb, or Ta[11,13] which acts as a donor when substituted for Ti. H_2 reduction of Cr-doped $SrTiO_3$[13] can also contribute to stabilizing Cr_{Ti}^{-}, because hydrogen is likely to become a shallow donor when doped in oxide semiconductors either at an interstitial site or at a substitutional oxygen site.[32] Wang *et al.*[12] studied the effects of the doping site by intentionally substituting Cr for Ti, $Sr(Ti_{0.95}Cr_{0.05})O_3$, and for Sr, $(Sr_{0.95}Cr_{0.05})TiO_3$. They found that higher oxidation states predominated in $Sr(Ti_{0.95}Cr_{0.05})O_3$, which is well consistent with our theory: the $Sr(Ti_{0.95}Cr_{0.05})O_3$ corresponds to the sample synthesized close to the $\mu = \mu_{Cr/Ti}$ condition in which the higher oxidation state of Cr_{Ti}^{0} is stabilized (Fig. 3(c)). Our theory rules out the existence of Cr_{Sr} in a high concentration under any plausible growth conditions. Thus, we believe that Cr_{Ti} predominates even in the $(Sr_{0.95}Cr_{0.05})TiO_3$ sample. Our interpretation is as follows. $(Sr_{0.95}Cr_{0.05})TiO_3$ was synthesized under the growth conditions in which the chemical potentials are close to $\mu = \mu_{Cr/Sr}$, thereby stabilizing Cr_{Ti}^{-} (Cr^{3+}) (Fig. 3(b)). The difference between the stable charge state of Cr_{Ti} in $Sr(Ti_{0.95}Cr_{0.05})O_3$ and $(Sr_{0.95}Cr_{0.05})TiO_3$ explains the superior photocatalytic activity of the latter, because Cr_{Ti}^{-} assists both

visible-light absorption and reduction of H^+ into H_2. In addition, Cr_{Ti}^{-} (Cr^{3+}) possesses a magnetic moment because the unpaired electrons exist in the t'_{2g} state (Fig. 1), and should be detected by the electron paramagnetic resonance measurement. Such experiments performed for reduced Cr-doped $SrTiO_3$ showed clear evidence of Cr_{Ti}^{-} (Cr^{3+}).[33] The magnetic moment in Cr-doped $SrTiO_3$ appears to be adjustable corresponding to the charge state of the Cr defect. Hence, our results also can be used as a guide to develop dilute magnetic wide band-gap semiconductors.

4. Conclusions

In summary, based on hybrid density-functional calculations, we found that the Cr impurity occupies the Ti site (Cr_{Ti}) preferentially over all other sites in $SrTiO_3$ under any equilibrium growth conditions. Our theory suggests that Cr_{Ti}^{-} plays a key role in visible-light absorption and the enhancement of photocatalytic activities of Cr-doped $SrTiO_3$. The desirable charge state can be stabilized by tuning the growth conditions, which influence the chemical potentials of each element and the Fermi level of the system. This concept should be widely applicable to the oxide semiconductors doped with multivalent transition-metals such as Cr-doped TiO_2[11] and Rh-doped $SrTiO_3$.[34]

Acknowledgements

This work was supported by the Japan Society for the Promotion of Science KAKENHI (21760030) and JST PRESTO program. P.R. and N.U. thank the High-Performance Computing Center of California NanoSystems Institute (CNSI, UCSB) and Synchrotron Light Research Institute (SLRI, Thailand) for their hospitality.

References

1 A. Fujishima and K. Honda, *Nature*, 1972, **238**, 37–38.
2 H. Tong, S. Ouyang, Y. Bi, N. Umezawa, M. Oshikiri and J. Ye, *Adv. Mater*, 2011, DOI: 10.10002/adma.20110275.
3 M. Miyauchi, A. Nakajima, T. Watanabe and K. Hashimoto, *Chem. Mater*., 2002, **14**, 2812–2816.
4 Y. Xu and M. A. A. Schoonen, *Am. Mineral*., 2000, **85**, 543–556.
5 M. S. Wrighton, A. B. Ellis, P. T. Wolczanski, D. L. Morse, H. B. Abrahamson and D. S. Ginley, *J. Am. Chem. Soc*., 1976, **98**, 2774–2779.
6 A. K. Ghosh and H. P. Maruska, *J. Electrochem. Soc*., 1977, **124**, 1516–1522.
7 K. Domen, S. Naito, T. Onishi, K. Tamaru and M. Soma, *J. Phys. Chem*., 1982, **86**, 3657–3661.
8 H. P. Maruska and A. K. Ghosh, *Sol. Energy Mater*., 1979, **1**, 237–247.
9 R. U. E. t Lam, L. G. J. de Haart, A. W. Wiersma, G. Blasse, A. H. A. Tinnemans and A. Mackor, *Mater. Res. Bull*., 1981, **16**, 1593–1600.
10 M. Matsumura, M. Hiramoto and H. Tsubomura, *J. Electrochem. Soc*., 1983, **130**, 326–330.
11 H. Kato and A. Kudo, *J. Phys. Chem. B*, 2002, **106**, 5029–5034.
12 D. Wang, J. Ye, T. Kako and T. Kimura, *J. Phys. Chem. B*, 2006, **110**, 15824–15830.
13 T. Ishii, H. Kato and A. Kudo, *J. Photochem. Photobiol., A*, 2004, **163**, 181–186.
14 J. W. Liu, G. Chen, Z. H. Li and Z. G. Zhang, *J. Solid State Chem*., 2006, **179**, 3704–3708.
15 M. Miyauchi, M. Takashio and H. Tobimatsu, *Langmuir*, 2003, **20**, 232–236.
16 J. Wang, S. Yin, M. Komatsu, Q. Zhang, F. Saito and T. Sato, *J. Photochem. Photobiol., A*, 2004, **165**, 149–156.
17 W. Wei, Y. Dai, H. Jin and B. Huang, *J. Phys. D: Appl. Phys*., 2009, **42**, 055401.
18 H. Raebiger, S. Lany and A. Zunger, *Nature*, 2008, **453**, 763–766.
19 Y. Matsumoto, M. Murakami, T. Shono, T. Hasegawa, T. Fukumura, M. Kawasaki, P. Ahmet, T. Chikyow, S.-y. Koshihara and H. Koinuma, *Science*, 2001, **291**, 854–856.
20 K. Sato, L. Bergqvist, J. Kudrnovský, P. H. Dederichs, O. Eriksson, I. Turek, B. Sanyal, G. Bouzerar, H. Katayama-Yoshida, V. A. Dinh, T. Fukushima, H. Kizaki and R. Zeller, *Rev. Mod. Phys*., 2010, **82**, 1633.
21 Y. Maeno, T. Tomita, M. Kyogoku, S. Awaji, Y. Aoki, K. Hoshino, A. Minami and T. Fujita, *Nature*, 1987, **328**, 512–514.
22 G. Kresse and J. Furthmüller, *Comput. Mater. Sci*., 1996, **6**, 15–50.
23 J. Heyd, G. Scuseria and M. Ernzerhof, *J. Chem. Phys*., 2003, **118**, 8207–8215.
24 J. P. Perdew, K. Burke and M. Ernzerhof, *Phys. Rev. Lett*., 1996, **77**, 3865.
25 K. Van Benthem, C. Elsässer and R. H. French, *J. Appl. Phys*., 2001, **90**, 6156–6164.
26 A. Janotti, J. B. Varley, P. Rinke, N. Umezawa, G. Kresse and C. G. Van de Walle, *Phys. Rev. B: Condens. Matter*, 2010, **81**, 085212.
27 A. Okazaki and M. Kawaminami, *Mater. Res. Bull*., 1973, **8**, 545–550.
28 J. Robertson, *Eur. Phys. J.: Appl. Phys*., 2004, **28**, 265–291.
29 A. Boonchun, M. F. Smith, B. Cherdhirunkorn and S. Limpijumnong, *J. Appl. Phys*., 2007, **101**, 043521–043527.
30 C. G. Van de Walle and J. Neugebauer, *J. Appl. Phys*., 2004, **95**, 3851–3879.
31 W. Tang, E. Sanville and G. Henkelman, *J. Phys.: Condens. Matter*, 2009, **21**, 084204.
32 S. Limpijumnong, P. Reunchan, A. Janotti and C. G. Van de Walle, *Phys. Rev. B: Condens. Matter*, 2009, **80**, 193202.
33 S. F. Alvarado, F. La Mattina and J. G. Bednorz, *Appl. Phys. A: Solid Surf*., 2007, **89**, 85–89.
34 K. Iwashina and A. Kudo, *J. Am. Chem. Soc*., 2011, **133**, 13272–13275.

